Supplementary Material for RESCUE: Crowd Evacuation Simulation via Controlling SDM-United Characters

Xiaolin Liu[1,†], Tianyi Zhou[1,†], Hongbo Kang[1], Jian Ma[1], Ziwen Wang[1], Jing Huang[1], Wenguo Weng[2], Yu-Kun Lai[3], Kun Li[1,*]
[1]Tianjin University, [2]Tsinghua University, [3]Cardiff University
{liuxiaolin, tianyizhou, hbkang, jianma, 3021244417, hj00, lik}@tju.edu.cn,
wgweng@tsinghua.edu.cn, Yukun.Lai@cs.cardiff.ac.uk
[†]Equal contribution [*]Corresponding author

1. Overview

In this document, we provide the following supplementary contents:

- The details of Personalized Optimization for SDM Coefficients (Sec. 2)
- Supplementary Algorithm: Personalized Optimization for SFM Coefficients (Sec. 3)
- Supplementary Algorithm: Personalized Optimization for SFM Coefficients (Sec. 4)
- Supplementary qualitative comparison (Sec. 5).
- Supplementary ablation study (Sec. 6).
- Stylized motion evaluation (Sec. 7).
- Quantitative experiment in motion diversity (Sec. 8).
- The details of user study (Sec. 9).
- Analysis of falling process during evacuation (Sec. 10).
- Limitations (Sec. 11).

2. Details of Personalized Optimization for SDM Coefficients

Table 1 shows the real escape speeds [1, 2, 4] and optimized driving force coefficients in social force model for the five categories of people in Section 3.3.

Table 1. Escape Speed and Self-drive Coefficient for Different Categories of People

People Categories	v_0	τ_{relax}	Survey Data(m/s)
the Young	5.75	0.498	2.37
the Middle-aged	4	0.492	1.69
the Old	2.625	0.501	1.07
Patients	3.25	0.5	1.340
the Disabled	2.5	0.506	1.00

3. Supplementary Algorithm: Personalized Optimization for SFM Coefficients

Algorithm 1 provides the detailed pseudocode for personalized optimization algorithm for SFM Coefficients described in Section 3.3 of the main paper.

Algorithm 1: Personalized Optimization for SFM Coefficients

Input: Input initial position of an agent p_0, simulation duration t_{sim}, real-world escape speed v_{sim}
Output: SFM coefficients v_0 and τ_{relax}
Initialize SFM coefficients v_0 and τ_{relax};
Simulate forward motion in physics engine using the social force model with the current coefficient v_0 and τ_{relax};
Get current position p_{cur};
$v_{\text{sim}} \leftarrow (p_{\text{cur}} - p_0)/t_{\text{sim}}$;
repeat
  $\tau_{\text{relax}}, v_0 \leftarrow \text{Update}(\tau_{\text{relax}}, v_0, v_{\text{sim}}, v_{\text{real}})$;
  Initialize SFM coefficients v_0 and τ_{relax};
  Simulate forward motion in physics engine using the social force model with the current coefficient v_0 and τ_{relax};
  Get current position p_{cur};
  $v_{\text{sim}} \leftarrow (p_{\text{cur}} - p_0)/t_{\text{sim}}$;
until $\text{abs}(v_{sim} - v_{real}) \leq 0.005\,m/s$;
return v_0 and τ_{relax};

4. Supplementary Algorithm: Gait Frame Matching

Algorithm 2 provides the detailed pseudocode for gait frame matching algorithm described in Section 3.4 of the

main paper.

Algorithm 2: Gait Frame Matching

Input: Unpersonalized motion frame set $\mathcal{F}_{\mathrm{g}} = [\mathbf{f}_{\mathrm{g},1}, \mathbf{f}_{\mathrm{g},2}, ..., \mathbf{f}_{\mathrm{g},N}]$, personalized motion frame set $\mathcal{F}_{\mathrm{p}} = [\mathbf{f}_{\mathrm{p},1}, \mathbf{f}_{\mathrm{p},2}, ..., \mathbf{f}_{\mathrm{p},M}]$

Output: Matching relation $\mathcal{R} \subseteq \mathcal{F}_{\mathrm{g}} \times \mathcal{F}_{\mathrm{p}}$

Initialize $\mathcal{R} \leftarrow \emptyset$;

Initialize gait values $\mathcal{V}_{\mathrm{g}} = [0]^N$ and $\mathcal{V}_{\mathrm{p}} = [0]^M$;

Compute ankle distance sequence $D_{\mathrm{g}} = [d_{\mathrm{g},1}, d_{\mathrm{g},2}, ..., d_{\mathrm{g},N}]$,$D_{\mathrm{p}} = [d_{\mathrm{p},1}, d_{\mathrm{p},2}, ..., d_{\mathrm{p},M}]$ of $\mathcal{F}_{\mathrm{g}}$,$\mathcal{F}_{\mathrm{p}}$;

Detect gait keyframes (peak, trough, peak, trough) in D_{g} and D_{p} based on local extrema;

According to the relative position of the feet, assign gait values $0, 0.3, 0.5, 0.75$ to these keyframes respectively.

Interpolate gait values to surrounding frames in $\mathcal{V}_{\mathrm{g}}$, $\mathcal{V}_{\mathrm{p}}$;

foreach $\mathbf{f}_{g,i} \in \mathcal{F}_g$ *and* $v_{g,i}$ **do**

  Define candidate set: $\mathcal{C}_i = \left\{\mathbf{f}_{\mathrm{p},j} \in \mathcal{F}_{\mathrm{p}} \,\middle|\, |v_{\mathrm{p},j} - v_{\mathrm{g},i}| = \min_{v \in \mathcal{V}_{\mathrm{p}}} |v - v_{\mathrm{g},i}|\right\}$;

  Compute the joint angles similarity between candidates and $\mathbf{f}_{\mathrm{g},i}$:
  $s_{i,j} = \mathrm{Sim}(\mathbf{f}_{\mathrm{g},i}, \mathbf{f}_{\mathrm{p},j}), \quad \forall \mathbf{f}_{\mathrm{p},j} \in \mathcal{C}_i$;

  Select the most similar frame:
  $j^* = \arg\max_j s_{i,j}$;

  Add matching pair to relation:
  $\mathcal{R} \leftarrow \mathcal{R} \cup \{(\mathbf{f}_{\mathrm{g},i}, \mathbf{f}_{\mathrm{p},j^*})\}$;

return $\mathcal{R}$;

5. Supplementary Qualitative Comparison

Figure 7 shows the evacuation processes and evacuation motions executed by the three comparison models and our framework on 2 classic evacuation scenarios as well as a large-scale scenario. Our approach achieves more rational evacuation processes and simulates personalized evacuation motions tailored to individuals with different attributes. We also test the recent methods TECRL [8] and tlcontrol [6] in our evacuation scenarios as shown in Figure 1 and 2 .

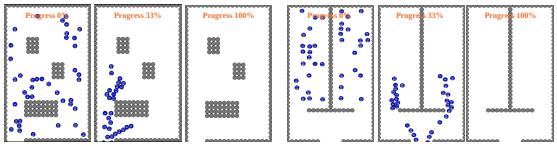

Figure 1. Qualitative results of TECRL.

6. Supplementary Ablation Results

We compare the pipeline of our framework after removing the 3D-adaptive SFM Decision Mechanism, the Personalizing Gait Control Motor, and both components together, which degrades into the PACER[3] baseline. Figure 8 shows the evacuation processes and evacuation motions on 2 classic evacuation scenarios. Our complete framework achieves more rational evacuation processes and simulates personalized evacuation motions tailored to individuals with different attributes.

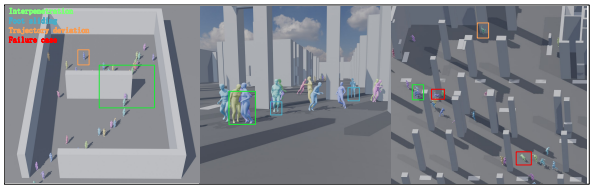

Figure 2. Qualitative results of TLControl.

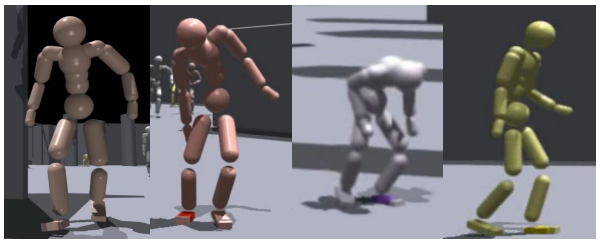

Figure 3. Stylization.

7. Stylized Motion Evaluation

We conducted an evaluation of the stylized motions using Style Recognition Accuracy (SRA)and obtained a score of 80.79%, and Figure 3 gives representative examples with style labels.

8. Quantitative Experiment in Motion Diversity.

Motion diversity quantifies the variability of motion embeddings across agents and scenarios, indicating the ability to generate dynamic and diverse behaviors. Table 2 compares the diversity scores. The generative method OmniControl [7] achieves greater diversity but often lack stability in multi-agent scenarios. MaskedMimic [5], the character control state-of-the-art (SOTA) method, produces actions that are overly uniform. Our method strikes a balance between controllability and diversity by integrating personalized action generation with stable control techniques. Hence, our approach surpasses MaskedMimic in diversity.

9. User Study

We conduct a user study with 128 participants spanning various age groups. The study comprises 17 questions rank-

Table 2. Diversity Comparison Across Methods

Method	Diversity (Mean ± Std)
MaskedMimic	1.01 ± 0.67
OmniControl	1.64 ± 1.13
Ours	1.32 ± 0.64

ing visual effects and 6 questions assessing contact judgment.

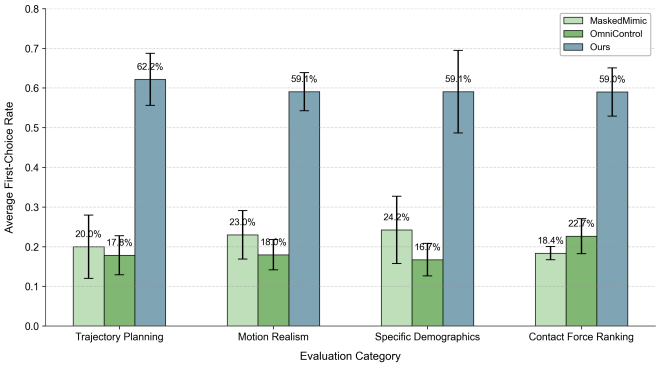

Figure 4. Comparisons of average first-choice rates with standard deviation.

As illustrated in Figure 4, the results of the ranking questions (Questions 1–17) underscore the proposed framework's superiority across multiple evaluation dimensions. Specifically, in trajectory planning and motion realism, our method achieves significantly higher average rankings (62.2% and 59.1%, respectively) compared to MaskedMimic (20.0%, 23.0%) and OmniControl (17.8%, 18.0%). The lower standard deviation further confirms the stability of these statistical outcomes. Notably, the framework excels in simulating specific demographics (59.1% best rate) and contacts force credibility (59.0%), validating the efficacy of our 3D adaptive SFM mechanism and personalized gait control in replicating diverse human behaviors.

For contact detection judgments (Questions 18–23), the visualization of component-level forces in the same scenario enables observers to more intuitively determine whether contact occurred between individuals. These results align with our technical contributions. The physics-aware decision-making process and attribute-driven motion generation enhance the realism of evacuation dynamics, particularly for vulnerable groups, while maintaining stable interactions in dense scenarios.

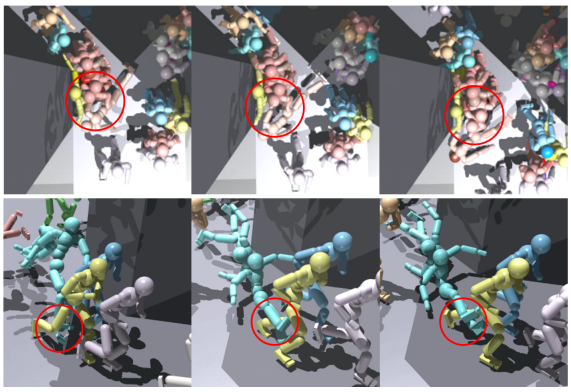

Figure 5. Visualizations of falls caused by pushing and limb entanglement in dense crowd scenarios.

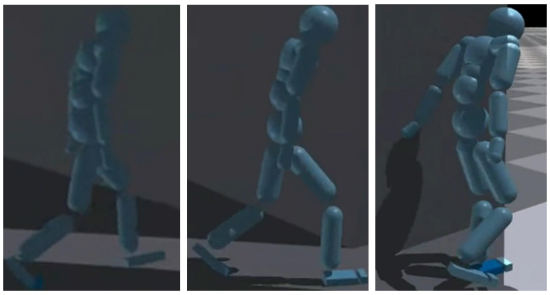

LimpLeft LimpRight LegsApart

Figure 6. Failure cases of personalized gait.

10. Analysis of Falling Process during Evacuation

Our simulation effectively captures the human falling due to collisions in dense crowd scenarios, providing realistic insights into evacuation dynamics. The experiments demonstrate the falls in evacuation scenarios predominantly. This would be due to two key factors: *pushing* caused by high crowd density and physical interactions, and *entanglement* arising from limb crossing in tight spaces. As shown in Figure 5, these results highlight the importance of modeling both physical forces and individual motion patterns.

11. Failure Cases and Limitations

When implementing personalized gait, lower body movements have a significant impact on gait stability and are limited by terrain. As a result, we are currently unable to personalize lower body gait that would allow us to simulate conditions such as limp and legsapart due to disabilities. We show some failure cases in Figure 6. Additionally, our simulation framework is currently limited to single-story escape scenarios and does not support multi-story scenarios.

References

[1] Mahdi Hashemi. 2018. Emergency evacuation of people with disabilities: A survey of drills, simulations, and accessibility. *Cogent Engineering* 5, 1 (2018), 1506304. 1

[2] VV Kholshevnikov, DA Samoshin, and AP Parfenenko. 2009. Pre-school and school children building evacuation. In *Proceedings of the Fourth International Symposium on Human Behaviour in Fire*. 243–254. 1

[3] Davis Rempe, Zhengyi Luo, Xue Bin Peng, Ye Yuan, Kris Kitani, Karsten Kreis, Sanja Fidler, and Or Litany. 2023. Trace and pace: Controllable pedestrian animation via guided trajectory diffusion. In *Proceedings of the IEEE/CVF Conference on Computer Vision and Pattern Recognition*. 13756–13766. 2

[4] Xiangxia Ren, Yanghui Hu, Hongliu Li, Jun Zhang, Weiguo Song, and Han Xu. 2022. Simulation of building evacuation with different ratios of the elderly considering the influence of obstacle position. *Physica A: Statistical Mechanics and its Applications* 604 (2022), 127833. 1

[5] Chen Tessler, Yunrong Guo, Ofir Nabati, Gal Chechik, and Xue Bin Peng. 2024. Maskedmimic: Unified physics-based character control through masked motion inpainting. *ACM Transactions on Graphics (TOG)* 43, 6 (2024), 1–21. 2

[6] Weilin Wan, Zhiyang Dou, Taku Komura, Wenping Wang, Dinesh Jayaraman, and Lingjie Liu. 2024. Tlcontrol: Trajectory and language control for human motion synthesis. In *European Conference on Computer Vision*. Springer, 37–54. 2

[7] Yiming Xie, Varun Jampani, Lei Zhong, Deqing Sun, and Huaizu Jiang. 2023. OmniControl: Control any joint at any time for human motion generation. *arXiv preprint arXiv:2310.08580* (2023). 2

[8] Zihan Yu, Guozhen Zhang, Yong Li, and Depeng Jin. 2023. Understanding and modeling collision avoidance behavior for realistic crowd simulation. In *Proceedings of the 32nd ACM International Conference on Information and Knowledge Management*. 3052–3061. 2

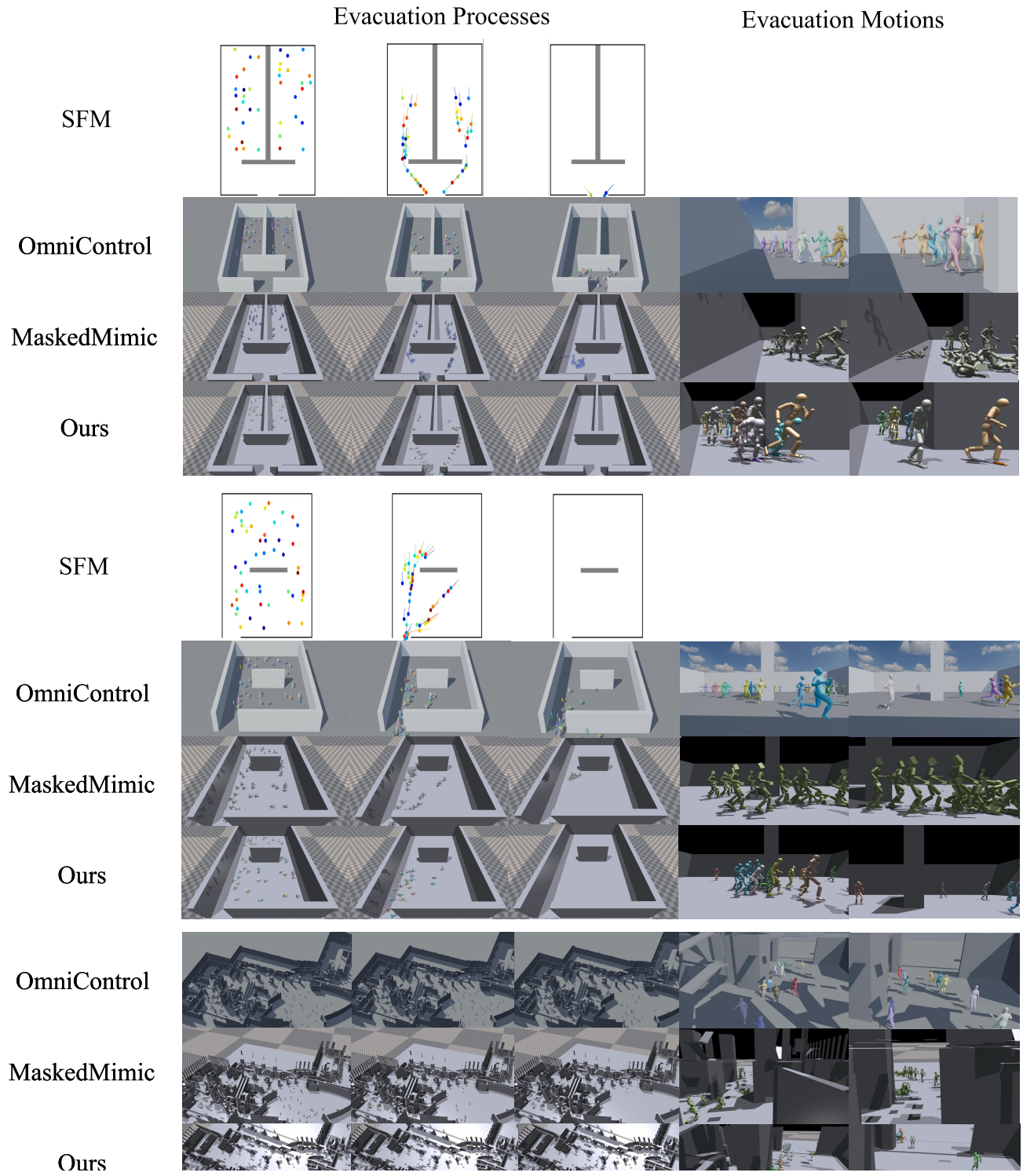

Figure 7. Qualitative comparison.

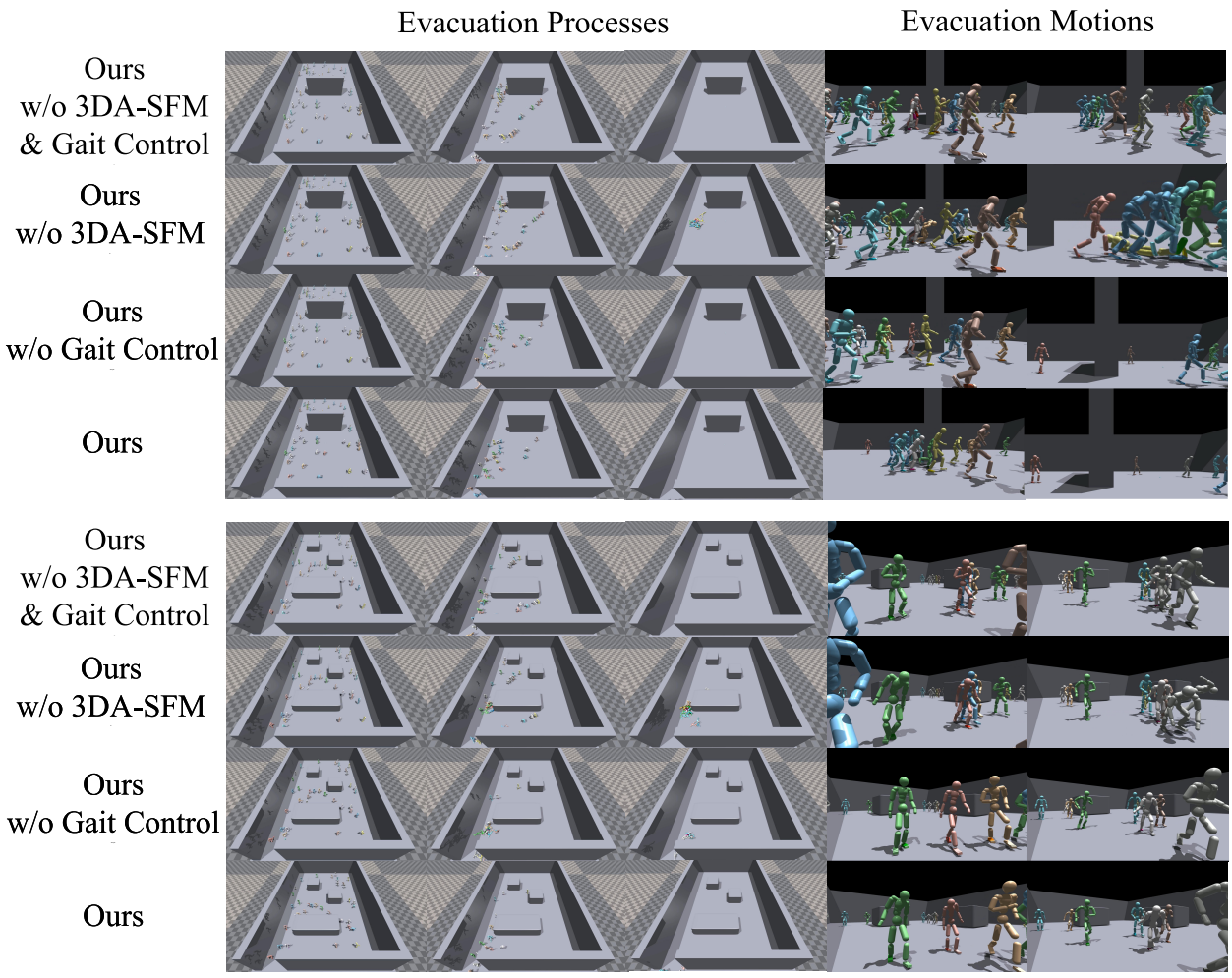

Figure 8. Ablation study results.